Benchmark Tests on Conventional Surface Potential Based Charge-Sheet Models And the Advanced PUNSIM Development

Jin He,Yan Song, Xudong Niu, Ganggang Zhang, Xing Zhang, Ru Huang, Mansun Chan*, and Yangyuan Wang

Institute of Microelectronics, EECS, Peking University, Beijing, 100871, P.R.China
*Department of EEE, Hong Kong University of Science & Technology, Clearwater Bay, Kewloon, Hong Kong
Tel: 86-10-62765916 Fax: 86-10-62751789 e-mail: jinhe@ime.pku.edu.cn

Abstract: This paper reports benchmark test results of some conventional surface potential-based models and PUNSIM development. The benchmark tests demonstrated that the conventional surface potential-based always exist some device physics, accuracy, and self-consistent issues for the inversion charge, channel current, surface potential prediction and the short-channel effect modeling. The advanced PUNSIM is developed to overcome drawbacks all mentioned above while aiming at fulfilling the features: physics based analytic solution of the surface potential; an accurate description of inversion charge; physics based channel current equation and calculation; Self-consistently modelling of shosrt-channel effects.

Keywords: CMOS technology， Device physics， Compact modeling, Surface potential-based model.

I. Introduction

In recent compact model formulations, considerable attention has been focused on developing surface potential based charge-sheet models [1-5]. This is due to some identified drawbacks in threshold voltage based models, such as the discontinuity across different operation regions, negative conductance and negative capacitance. A number of surface potential based compact models [6-10] have been developed based on J.R.Brews's charge-sheet model with the claiming that such a model retains the fundamental physics with high accuracy and continuity. Moreover, some surface potential based model such as PSP and HISIM use so-called bias and geometry dependent lateral gradient factor to model all short-channeled effects in the surface potential equation with the claim to goes beyond the gradual channel approximation. The core of these models consists of the surface potential equation, inversion charge equation, channel current equations, and short-channel effects related equations. Thus, this paper reports the benchmark test results of the surface potential, inversion charge and the channel current calculation of various surface based charge-sheet models for an ideal long channel MOS devices for the sake of simplicity. At the same time, the short-channel effects related surface potential equation is also analyzed theoretically and demonstrated its drawbacks of insistence in predicting short-channel effects from the results of PSP and HISIM.

First basic issue of the surface potential based models is that there is no a first principle surface potential equation to ensure surface potential correct calculation physically and numerically. Thus, various modification surface potential equations have been proposed [11-13]. At the same time, the common problem of the existing closed-form approximations for the surface potential solution is the need for dropping hole-related terms off above the flat-band while neglecting the electron related terms below the flat-band region [7-8]. This kind of the simplification does not only degrade the accuracy of the surface potential calculation, but also results in poor prediction of the trans-capacitances. Moreover, they give the incorrect result for the forward bias source and drain ends. On the other hand, although the iterative method can give the exact surface potential value, it leads to the complex solution close the flat-band region and efficiency depends on the steps and process parameters.

Compared with the result from the Pao-Sah model [1], a classical model that retains all the essential basic physics of a 1-D ideal long MOSFET but needs the complex double integral for the current calculation, most charge-sheet models produce different degrees of difference in the inversion charge calculation. Some approximations even display an incorrect trend in the sub-threshold region.

The difference in channel current calculation is more prominent compared with the Pao-Sah model, mainly coming from the semi-empirical characteristics of the charge-sheet current equation, which is not consistent with the inversion charge formulation. We will discuss from the perspective of the device physics that the sum of the drift and diffusion currents in a charge-sheet current equation is not exactly equal to the total current of Pao-Sah model to obtain from the product of the carrier density and the gradient of the quasi-Fermi potential. Thus, the resultant channel current of the charge-sheet model is always less than exact value predicted by the Pao-Sah model for the same bias and parameters.

By using the bias and geometry dependent lateral gradient factor to model short-channel effects, the surface potential based models such as PSP and HISIM claim that they go beyond the gradul channel approximation simplification. However, the deeply theoretical analysis and numerical tests demonstrate such a method only correctly describes threshold voltage roll-off. It, however, also results in the decrease of the sub-threshold slope with the decrees of the channel length and Vds increase, a picture inconsistent with the device physics. TI and Philips's evaluation on HISIM and PSP also verified their non-physical characteristics and difficulty in fitting the sub-threshold region of short-channel devices.

All these analyses demonstrate that the conventional surface potential based charge-sheet models still require more improvement to retain the fundamental physics characteristics and the high accuracy of the Pao-Sah model in addition to a precise surface potential being obtained analytically or numerically. Under such a background, the PUNSIM is developed to overcome mainly drawbacks of the presented

surface potential based models and aiming at fulfilling the features: The first-principle derivation of the complete surface potential equation; Physics based analytic solution of the surface potential equation; Accurate description of inversion charge; Physics based channel current equation and calculation; Self-consistently modelling of short-channel effects.

II. Benchmark tests on surface potential calculation

The device physics of MOSFET starts with the Poisson's equation and its resultant normalized surface potential equation

$$v_G - x = G\sqrt{x + e^{-x} - 1 + e^{-2x_f - x_n}\left[e^{x} - xe^{x_n} - 1\right]} \quad (1)$$

In the recent publication [11], the authors made two clever statements. First, they showed that the argument in the square root of (1) becomes negative when $x_n \neq 0$ and x is near and at zero. This result demonstrates there exists a physics, thus a numerical problem with the solution of (1) in a region where x is near and at zero. It is generally thought that this flaw does not affect the output characteristics of MOS transistors but are essential for the convenience of compact modeling work [12]. In fact, the negative range of the square root of (1) not only depends on the magnitude of doping concentration for constant x_n as shown in Fig.1(a), it also results in a discontinuity gate capacitance region as shown in Fig.1(b) for different x_n, thus, definitely affect the output characteristics. In such case, it is a basis to develop the complete surface potential equation for the compact modeling.

Secondly, the authors made a mathematic modification of $xe^{x_n} \equiv x$ avoid the numerical problem. We think this is only a mathematic yet better modification for the correct surface potential calculation.

In order to fix this flaw, the PSP authors proposed the new modification

$$v_G - x = G\sqrt{x + e^{-x} - 1 + 2e^{-2x_f - x_n}\left[\sinh(x) - x\right]} \quad (2)$$

For bulk MOSFETs [12] and

$$v_G - x = G\sqrt{x + e^{-x} - 1 + e^{-2x_f - x_n}\left[e^{x} - x - 1 - x^2/(2 + x^2)\right]} \quad (3)$$

For SOI MOSFETs [13].

All these modifications only consider the mathematic conditions for the surface potential calculation rather than a physical derivation. In fact, PSP all modifications have non-physical derivative issue passing the flat-band point if a careful test is made. We would like to stress that the Poisson's equation solution and its variations with the different boundary conditions can be derived from the first principle of the MOSFET device physics and it is continuous in all operation, thus, works well either for bulk MOSFET or Silicon-on-Insulator (SOI), Ultra-Thin-Body (UTB) devices. A unified and physics based surface potential equation of a MOSFET must be resorted for bulk and non-classical MOSFET, and any artificial modification and addition should be thought a bad mathematic trick rather than the physics-based effort. Fortunately, PUNSIM model already obtained a first principle derivation of the complete surface potential equation and its result is shown in (4)

$$v_G - x = G\sqrt{x + e^{-x} - 1 + e^{-2x_f - x_n}\left[e^{x} - x - 1\right]} \quad (4)$$

Most of the problems with existing analytic approximations of the surface potential solution were related to dropping off the hole related terms above the flat-band point and electron related terms below the flat-band region. The resulting errors are demonstrated in this section using the well-known MOS-11 from Philips [5-6] and original SP model from Pennsylvania State University [7-8], compared with the numerical results of (3) acting as the benchmark test reference.

The analytic approximation of MOS-11 starts from a simplified surface potential equation [5-6].

$$v_G - x = G\sqrt{x + e^{x - x_n}} \quad (5)$$

It is evident that (5) drops off four related items compared with (4), which has the different effects on the calculation of the surface potential and trans-capacitance calculation. It is this simplification that makes the first initial be obtained from (5) by neglecting the exponential term and then second smooth function is used to link the sub-threshold and linear region. On the other hand, the original analytic approximation of SP starts from another simplified surface potential equation [8]

$$v_G - x = G\sqrt{x - 1 + e^{x - x_n}} \quad (6)$$

Compared with (4), SP model also drops off at least three related items. It is such a simplification that makes the SP analytic algorithm work, e.g. it uses the Taylor expanding, to deliver a so-called accuracy of better than 1 nV. Similar, (6) can be used to demonstrate the problem SP model has around the near flat-band bias point.

Fig.2 (a) demonstrates the comparison of the normalized surface potential calculation between (4), MOS-11, (4) and SP, (6). It seems there is no difference because three match well in whole operation region. However, this is only in a relatively large scale. In fact, (5) of MOS-11 always has several thermal voltage difference in the whole sub-threshold region but it always approaches zero as (4) does demonstrate while (6) of SP model having a good match in the most bias region but it starting to demonstrate some errors when the effective gate voltage is beyond five times thermal voltages and not approaching zero close to the flat-band region as the physics based model does require, as shown in Fig.2(b) for an enlarged result for the region close to the flat-band region.

The trans-capacitance calculation, e.g. the partial derivative of the surface potential with respective to the terminal bias is a more stringent test for various surface potential approximations. The comparison of the space charge layer capacitance calculation coming from (5), MOS-11 and (6) of the original SP is shown in Fig.3. One can find that relatively small difference of the surface potential calculation can result in relatively large errors of the space charge layer capacitance calculation. Clearly, the difference of the space charge layer capacitance becomes evident once the effective gate voltage is less the threshold voltage for the MOS-11 and several hundreds of mV for the original SP method. Final issue of the original SP and MOS-11 is that they result in large error in the surface potential calculation for forward body bias, as shown in Fig.4. We also note that the latest code of the PSP model uses other smooth function to handle this high error region by building the section solution of the surface potential above the flat-band region [14]. This algorithm still has non-physical results for the forward body bias and discontinuity for low doping concentration [15-16] as shown Fig.13.

III. Benchmark tests on inversion charge calculation

Since the Pao-Sah model acts as the reference benchmark, the inversion charge of the Pao-Sah model is also calculated numerically following an integration definition.

$$q_m = \int_0^{\phi_s} \frac{\sqrt{2qN_a\varepsilon_{si}}\exp\left(\frac{\phi-2\phi_F-V_{ch}}{\phi_t}\right)d\phi}{\left[\phi_t\exp\left(-\frac{\phi}{\phi_t}\right)+\phi-\phi_t+\exp\left(-\frac{2\phi_F+V_{ch}}{\phi_t}\right)\left(\phi_t\exp\left(\frac{\phi}{\phi_t}\right)-\phi-\phi_t\right)\right]^{1/2}} \quad (7)$$

We first test the inversion charge from the depletion approximation because this charge-sheet approximation was used in another version of the J.R.Brew's charge-sheet model [3], some standard text books [5] and original MOS-11[7]

$$q_m = C_{ox}\left(V_{GB}-V_{FB}-\phi_S\right)-\gamma C_{ox}\sqrt{\phi_s} \quad (8)$$

From the numerical surface potential, the inversion charge comparison between equation (3) and the Pao-Sah model for the different Quasi-Fermi-Potential is shown in Fig.5. The right of Fig.5 illustrates that the inversion charge from (8) is negative in the sub-threshold region, thus it cannot be plotted in the logarithmic curve. Instead, a linear-scale is used to demonstrate the magnitude as shown in the left of Fig.5.Since the result is incorrect from the perspective of device physics, this approximation cannot produce an accurate compact model although the popular text books use it.

The second test objective is to study the inversion charge calculation based on classical charge-sheet approximation [2].

$$q_m = C_{ox}\left(V_{GB}-V_{FB}-\phi_S\right)-\gamma C_{ox}\sqrt{\phi_s-\phi_t} \quad (9)$$

The resultant inversion charge comparison with the Pao-Sah model is shown in Fig.6. This charge-sheet approximation results in an increase of the inversion charge with the decrease of the surface potential in the weak inversion region. Please note that (9) is ever used by original SP and HISIM to calculate the inversion charge.

The latest released MOS-1102 [6], latest PSP [9], and HISIM [10] recently used one inversion charge equation based on a modified charge-sheet model

$$q_m = C_{ox}\left(V_{GB}-V_{FB}-\phi_S\right)-\gamma C_{ox}\sqrt{\phi_s-\phi_t\left[1-\exp\left(-\phi_s/\phi_t\right)\right]} \quad (10)$$

The resultant inversion charge comparison with the Pao-Sah model is shown in Fig.7. In contrast with (8) and (9), the inversion charge predicted by (10) shows a very good match with the Pao-Sah model in most surface potential regions. However, it still displays a little difference in the far weak-inversion region that may lead to some errors in the off-current prediction as shown in the inset of Fig.7.

Once (10) is used, a serious issue for compact models is that no closed-form current expression for IV modeling and partition charge expression for CV modeling can be obtained as (10) cannot be integrated analytically. For example, the drift current component inside the charge-sheet current equation

$$I_{ds(drift)} = q\mu W q_m\frac{d\phi_s}{dx} = q\mu W C_{ox}\left[\left(V_{GB}-V_{FB}-\phi_S\right)-\gamma\sqrt{\phi_s-\phi_t\left[1-\exp\left(-\phi_s/\phi_t\right)\right]}\right]\frac{d\phi_s}{dx} \quad (11)$$

cannot result in a closed-form analytical expression. Similarly, the bulk charge component for the CV model

$$Q_B = \int q_b d\phi_s = \int C_{ox}\gamma\sqrt{\phi_s-\phi_t\left[1-\exp\left(-\phi_s/\phi_t\right)\right]}d\phi_s \quad (12)$$

also cannot give a closed-form analytical expression.

In this case, some compact models such as SP and MOS-11 have to use the so-called "linearization of the inversion charge" or "symmetric linearization method" to avoid this dilemma [17]. However, they are all additional approximations over the charge-sheet model and definitely result in some errors compared with the Pao-Sah model [18] as shown in Fig.8.

IV. Benchmark tests on channel current calculation

The classical charge-sheet current equation including the diffusion and drift components is written as

$$\frac{I_{ds}}{q\mu W} = \left[q_m\frac{d\phi_s}{dx}-\phi_t\frac{dq_m}{dx}\right] \quad (13)$$

As stated in [19], this charge-sheet current equation introduced an empirical term to account for diffusion current. Thus, it was not physics based but the approach is justified because it succeeded in producing "correct' I-V curves compared with the Pao-Sah model as stated in [2]. This equation is still an approximation although J.R.Brews finally gave a derivation in the later charge-sheet version [3] based on the additive assumption.

The physics based current formulation from the Pao-Sah model is written as

$$\frac{I_{ds}}{q\mu W} = q_m\frac{dV_{ch}}{dx} \quad (14)$$

Seemingly, if we equate (13) and (14), an equation between the inversion charge, surface potential and quasi-Fermi-potential is obtained

$$q_m\frac{d\phi_s}{dx}-\phi_t\frac{dq_m}{dx} = q_m\frac{dV_{ch}}{dx} \quad \Leftrightarrow \quad q_m = q_0\exp\left[\frac{\phi_s-V_{ch}}{\phi_t}\right] \quad (15)$$

(15) implies that the inversion charge is always an exponential function of the surface potential with constant slope of unity based on (13). However, the device physics [5] predicts the inversion charge versus the surface potential plot has an exponential slope of unity in the sub-threshold region and one-half in the strong inversion region as demonstrated in Figs.4-6, respectively.

We will discuss from the perspective of the device physics that the sum of the drift and diffusion currents in a charge-sheet current equation (13) is not exactly equal to the total current of Pao-Sah model (14) to obtain from the product of the carrier density and the gradient of the quasi-Fermi potential. From (1) and (10), it is easy to obtain

$$q_m = \frac{\gamma\exp\left(-\frac{2\phi_F+V_{ch}}{\phi_t}\right)\left[\exp\left(\frac{\phi_s}{\phi_t}-\phi_s-\phi_t\right)\right]}{q_m+q_b} \quad (16)$$

For conditions above flat-band region, the terms $-\phi_s-\phi_t$ in (16) are totally negligible, and we write

$$q_m = \frac{\gamma\exp\left(-\frac{2\phi_F+V_{ch}}{\phi_t}\right)\exp\left[\frac{\phi_s}{\phi_t}\right]}{q_m+q_b} \quad (17)$$

Setting or defining

$$T = q_m+q_b \quad \eta_{\phi_s} = \frac{1}{T}\frac{\partial T}{\partial\phi_s} \qquad \eta_{V_{cs}} = \frac{1}{T}\frac{\partial T}{\partial V_{ch}} \quad (18)$$

Then we obtain the detail form of the Pao-Sah current (14) in terms of the surface potential and inversion charge from (17)

$$q_m\frac{dV_{ch}}{dx} = q_m\frac{d\phi_s}{dx}-\phi_t\frac{dq_m}{dx}-q_m\left[\eta_{\phi_s}\frac{d\phi_s}{dx}+\eta_{V_{ch}}\frac{dV_{ch}}{dx}\right] \quad (19)$$

It is evident that the current equation (13) of the charge-sheet model only includes the first two terms of the detail Pao-Sah current equation (19) and the last two terms in (14) are missed. If (13) is used to numerically calculate the channel current, the resultant channel current will always be

less than the exact value predicted by the Pao-Sah model following (14) even with the inversion charge from (10). Of interest is a comparison of the final I-V curve. Such a comparison of the normalized current is shown in Fig.9, where the circle curve is the charge-sheet model (13) and the square is the Pao-Sah model (14). For example, the error of the normalized channel current between (13) and (14) is about 5% for doping $10^{16}\,cm^{-3}$ and about 10% for $10^{17}\,cm^{-3}$, respectively. This kind of difference may be important when comparisons between the different compact models are made.

V. Benchmark tests on Short-channel effect modeling

The lateral field gradient, an attractive approach to treat small geometry effects was originated with [20] and then applied to compact modeling in HSIM and PSP model using geometry-dependent lateral field gradient approximation and further the essential bias dependence was introduced. To derive further analytical equations required for circuit simulation, different semi-empirical lateral field gradient expression introduces based on a parabolic potential distribution along the channel. The detail examples may refer to MISNAN, HISIM and PSP models. Here, we first analyzed the inconsistence of the short-channel effects predicted by the lateral field gradient from the basic device physics and then demonstrate the detail inconsistent results of the PSP and HISIM models.

In the present surface potential based models, the short channel effects were included in a quasi 1-dimensional Poisson equation.

$$v_G - x = G\sqrt{f(x-1)+e^{x-x_n}} \tag{20}$$

f is a semi-empirical lateral field gradient equation and it has the different forms in the different models. It, however, should show the general correct trend to decrease with the decrease of the channel length and the increase of Vds. Thus, the follow approximation capture the similar trend of the PSP and HISIM's lateral gradient equations, thus it can represent the general functionality PSP and HISIM's lateral gradient

$$f = 1 - F\left(V_{ds,}L, N_a, V_{bi}\right) \approx 1 - \frac{\alpha v_{ds}}{L^2} \tag{21}$$

Since the short-channel effects include the threshold voltage roll-off, sub-threshold slope increase and the DIBL enhancement, we can obtain the expressions of these variables from the first-order approximation, respectively.

In this case, the threshold voltage is approximated as

$$v_T = v_{fb} + x + G\sqrt{f(x-1)} \approx v_{fb} + 2x_f + G\sqrt{f(2x_f - 1)} \tag{22}$$

And the sub-threshold swing is expressed as

$$n = \frac{\partial v_G}{\partial \phi_S} = 1 + \frac{G\sqrt{f}}{2\sqrt{x-1}} \approx 1 + \frac{G\sqrt{f}}{2\sqrt{2x_f - 1}} \tag{23}$$

It is evident that the less the channel length, the less the factor f from (21), thus the threshold voltage will be rolled-off from (22). This result demonstrates the lateral field concept can capture the threshold voltage change. However, the less the factor f from (21), the sub-threshold swing of MOSFETs will reduce from (23). This result implies that the less the channel length of the MOSFETs, the less the sub-threshold swing. It is evident that this result is inconsistent with the basic device physics where the short channel MOFET results in a worse sub-threshold swing.

From recent result of PSP model on the SCE modeling as shown in Fig.10 [21], it is easily found that the lateral gradient concept is not sufficient to model short-channel effects of MOSFETs. The recent test result of TI on PSP model fitting to 90nm technology also demonstrated that PSP model cannot fit short-channel devices well in the sub-threshold region. We do believe that all these are directly related to the incorrect short-channel effect modeling approach of the PSP model.

On the other hand, the well-known figure of HISIM on DIBL effects as shown in Fig.11 also has the similar issues. According to (21), the larger the Vds, the less the factor f from (21), thus the threshold voltage will be rolled-off from (22). This result demonstrates the lateral field concept can capture the correct DIBL effect. However, the less the factor f from (21), the less the sub-threshold swing of MOSFETs from (23). This result implies that the larger the Vds, the better the sub-threshold swing. It is evident that this result is inconsistent with the basic device physics picture where the high Vds of the MOFET results in a worse sub-threshold swing. The recent test result of TI on HSIM model fitting to 90nm technology also demonstrated that HISIM model cannot fit short-channel devices well in the sub-threshold region as well as the PSP model.

VI. Advanced PUNSIM development

The advanced Peking University Nano-scale IGFET Model (PUNSIM) has been developed in EECS of Peking University to provide physics based solution scheme to the MOSFET modeling so as to overcome all drawbacks of the conventional surface potential based charge-sheet models. The main features of the PUNSIM are as follows: (1) The first principle derivation of the complete MOSFET surface potential equation; (2) A physics based analytic solution for the surface potential equation; (3) Physics based channel current equation and calculation; (4) Self-consistently modelling of short-channel effects; (5) Unique parameter scaling technology to ensure the high accuracy parameter extraction.

First-principle derivation of the complete MOSFET surface potential equation in the PUNISM:

In fact, once exists the non-zero channel voltage, no does exist the real equilibrium neutral condition even the surface potential equals to zero, as pointed out by Y.Tsividis [5]. Since $\phi = 0$ defines the free carrier equilibrium state of MOSFET either at the surface or in the deep bulk although $x_n \neq 0$ makes the n+p junction is in non-equilibrium, we can follow the complete Boltzmann statistics to construct a quasi- carrier equilibrium condition to fix the physics flaw, thus a numerical problem. Following this idea, we can derive the complete MOSFET surface potential equation from the first principle. To conclude, one must take into account that the commonly accepted and used surface potential equation dos not allow accurate and continuous modeling of the surface potential as

well as the charges and capacitance when you construct the surface-potential-based compact modeling of MOSFETs.

A physics-based analytic solution for the surface potential in the PUNSIM:

A physics-based analytic solution to the surface potential from the accumulation to the strong inversion region has been derived from complete MOSFET surface potential equation in the PUNISM model [16] without any need for the smooth and auxiliary functions, and its high accuracy in prediction of the surface potential in various conditions and the trans-capacitance has also been verified. Such an explicit surface potential solution not only leads us to deep understanding of MOSFET device physics, but also can be adopted as a basis for the advanced surface-potential-based model development. The comparison of the surface potential prediction between PUNISM and PSP is shown in Fig.12. In contrast, PSP code cannot pass this doping concentration scaling test as shown in Fig.13. Compared with the traditional surface potential iterative computations based on the computer source and the analytic approximations based on various smooth and auxiliary functions, we can expect the physics based analytic solution to the surface potential will definitely improve compact model computation efficiency for the circuit simulation and push deep understanding on the MOSFET device physics.

Physics based channel current equation in the PUNSIM:

Since the standard diffusion-drift current expression of the charge-sheet model (13) is a semi-empirical equation that missed some terms compared with the Pao-Sah model and is not consistent with the inversion charge equation, a physics-based current equation is developed in the PUNISM model for physics-based description of the MOSFET behaviour. This physics-based yet analytic equation is derived:

$$\frac{I_{ds}}{q\mu W} = \left[q_m \frac{d\phi_s}{dx} - \phi_t \frac{dq_m}{dx} - q_m \frac{d\ln\left[v_{gb} - v_{fb} - \phi_s\right]}{dx} \right] \qquad (24)$$

Self-consistently modelling of small size effects in the PUNSIM:

The 2-D Poisson equation is a general expression of electrostatics, linking the electrostatics to the doping and charge concentration. In PUNSIM model, a more general quasi 2-D method is used to get the 2-D solution of the Poisson equation. Since the short channel effect comes from the source and drain field penetrates into the total channel and terminated by the charges under the gate, it is well reasonable that the average value of the lateral field along the channel as the evaluated quantity of short-channel effects. This treatment greatly simplifies the calculation and related expressions. As a result, a consistent modeling approach for the short-channel effects including the threshold voltage rolling-off, the sub-threshold swing degradation and the DIBL effect is obtained. The general equation including SCEs and DIBL effect is used to combine with Pao-Sah current formulation to develop general channel current expression. This method is also valid for treatment of the narrow width device and non-uniform doping in the lateral direction.

Unique parameter scaling technology to ensure the high accuracy of parameter extraction in the PUNSIM:

Since the physics–based model of the MOSFETs requires a single set of the parameters and the equations for the different bias, geometry and temperature conditions, the physics-based scaling technology is highly preferred to ensure the accurate parameter extraction. The present several compact modelling represents such as BSIM3/4, HISIM, and PSP can only obtain the limited parameter extraction accuracy, for example, the extracted threshold voltage has errors about 20-30mV[23]. The ITRS requirement for such a quantity is far beyond these good results [24]. In order to follow the ITRS, the PUNSIM model develop the unique parameter scaling and extraction technology to ensure the high accuracy of the parameter extraction, e.g., extracted VT has error less 10 mV.

Acknowledgement:

This work is subsided by the special funds for major state basic research project and nature science funds of China. This work is also partially support by a competitive Earmarked Grant HKUST6289/04E from the Research Grant Council of Hong Kong SAR.

References

[1] H. C. Pao and C. T. Sah, *SSE*, vol. 9, pp. 927-937, 1966.
[2] J.R.Brews. *SSE,* vol.21, pp.345-352, 1978.
[3] J.R.Brews. Physics of the MOS transistor, Applied Solid State Science, Sup.2A, Academic Press Inc., p.1- 119, 1981.
[4]Y.P.Tsividis. Operation and modeling of the MOS transistor. New York: McGraw-Hill, 1999.
[5] A.R.Boothroyd, IEEE T-CAD, vol.10, pp.1512-1528, 1991.
[6]MOS11, http://www.semiconductors.Philips.com.
[7] R.V.Langevelde, et al., SSE, vol.44, pp.409-418, 2000.
[8] T.L.Chen et al., SSE, vol.45, pp.335-339, 2001.
[9] PSP model webste: http://pspmodel.ee.psu.edu.
[10] HISIM model, http://www.starc.jp.
[11] C.C.McAndrew, et al., IEEE TED-49, pp.72-81, 2002.
[12] W.Wu et al., IEEE TED-51, pp.1196, 2004.
[13] W. Wu, et al., IEEE CICC, pp. 819-822, 2005.
[14] G. Gildenblat, et al., IEEE JSSC, 39, 1394, 2004.
[15] HISIM team report, "Important features of HISM and comparison with PSP." Nov.10, 2005. CMC website: http://www.eigroup.org/CMC.
[16] Jin He, et al., Submitted for IEEE TED.
[17] J. Watts, etc. Workshop on Compact Modeling, NSTI-Nanotech, May, 2005.
[18] R.Rios, Internal communication on reviewing" Advanced compact models for MOSFETs".
[19] B.B.Jie, C.T.Sah, ICSICT'2004, D1.3, Oct.18-21, Beijing.
[20] T. Nguen and J. Plummer, IEDM, 1981, p. 596.
[21] T.L.Chen et al., SSE, vol.49, pp.335-339, 2005.
[22] TI Evaluation of the PSP and HiSIM Models, CMC website.
[23] CMC: http://www.cmc.org.
[24] ITRS, http://www.itrs.net/Common/2004Update

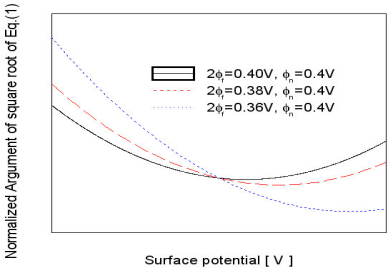

Fig.1 (a) Negative issue of square root term of Eq. (1) for different body doping concentration.

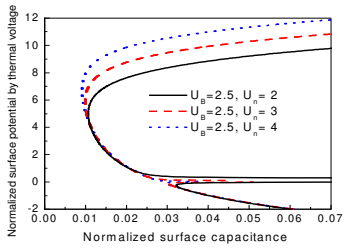

Fig.1 (b) Discontinuity issue of gate capacitance from (1)

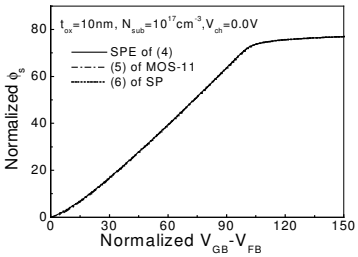

Fig.2 (a) Comparison of the surface potential calculation between (4), (5) of MOS-11 and (6) of SP.

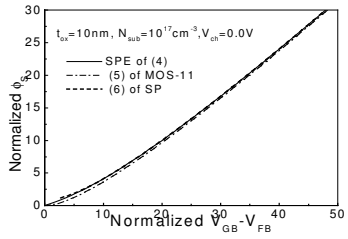

Fig.2 (b) Refined detail comparison of (4), (5) of MOS-11 and (6) of SP.

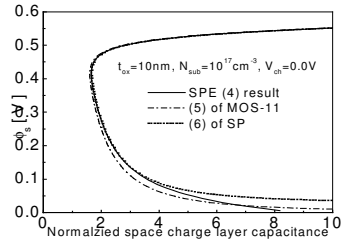

Fig.3 Comparison of the space charge layer capacitance calculation based on (4), (5) and (6).

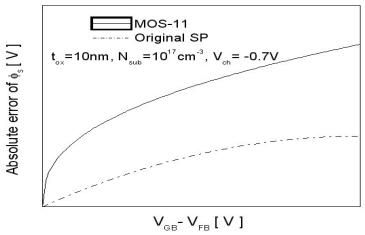

Fig.4 Surface potential evaluation error of MOS-11 and SP for the forward body bias.

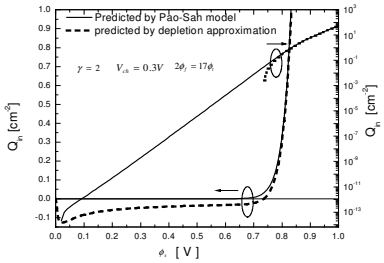

Fig.5 Inversion charge comparison between (8) and Pao-Sah model (7).

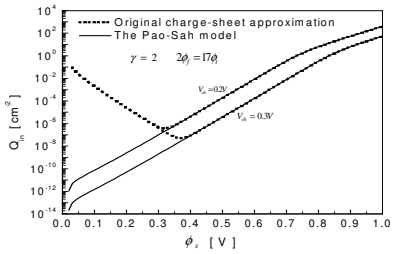

Fig.6 Inversion charge comparison between (9) and Pao-Sah model (7).

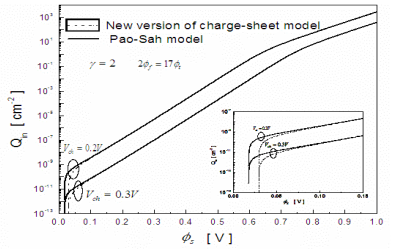

Fig.7 Inversion charge comparison between (10) and Pao-Sah model (7).

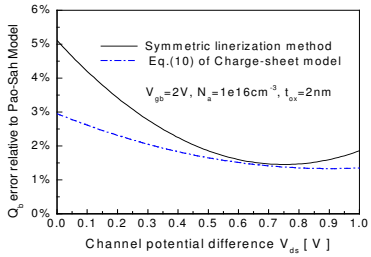

Fig.8 The bulk charge errors of the symmetric linearization method relative to numerical Pao-Sah model.

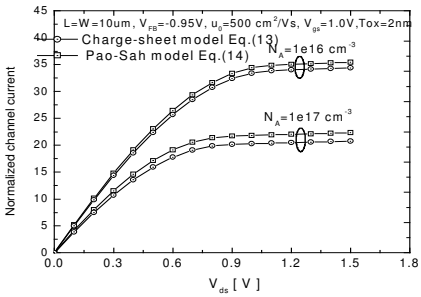

Fig.9 Normalized I_{ds}-V_{ds} curve comparison between the charge-sheet model and Pao-Sah model.

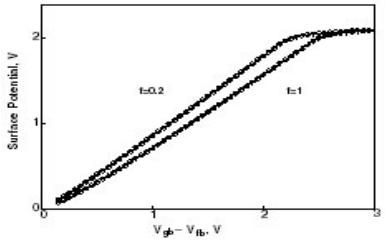

Fig.10 Simulated surface potential comparison with PSP including SCEs.

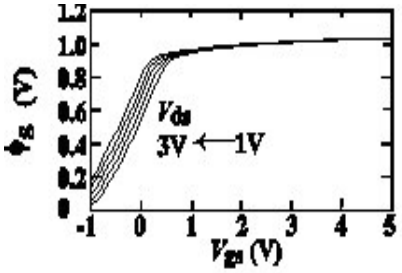

Fig.11 Simulated surface potential values with HiSIM including SCEs.

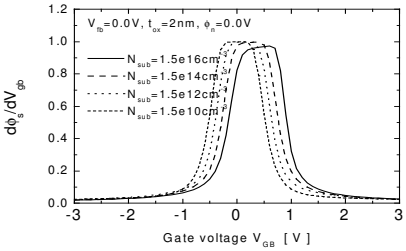

Fig.12 Gate capacitance scaling calculation in the PUNSIM code.

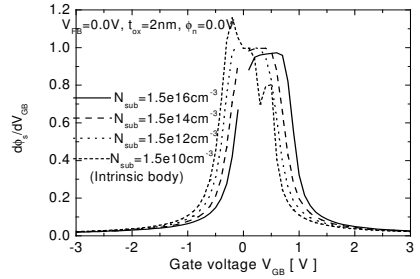

Fig.13 Gate capacitance scaling calculation based on the PSP code.